Distant ionospheric photoelectron energy peak observations at Venus

A.J. Coates [a,b,*], A. Wellbrock [a,b], R.A. Frahm [c], J.D. Winningham [c], A. Fedorov [d], S. Barabash [e], R. Lundin [e]

[a] Mullard Space Science Laboratory, University College London, Holmbury St Mary, Dorking RH5 6NT, UK
[b] Centre for Planetary Sciences at UCL/Birkbeck, Gower Street, London WC1E 6BT, UK
[c] Southwest Research Institute, San Antonio, TX 78228, USA
[d] Institut de Recherche en Astrophysique et Planétologie, 9, avenue du Colonel Roche, B.P. 4346, 31028 Toulouse Cedex 4, France
[e] Swedish Institute of Space Physics, Box 812, S98 128 Kiruna, Sweden

ABSTRACT

The dayside of the Venus ionosphere at the top of the planet's thick atmosphere is sustained by photoionization. The consequent photoelectrons may be identified by specific peaks in the energy spectrum at 20–30 eV which are mainly due to atomic oxygen photoionization. The ASPERA-4 electron spectrometer has an energy resolution designed to identify the photoelectron production features. Photoelectrons are seen not only in their production region, the sunlit ionosphere, but also at more distant locations on the nightside of the Venus environment. Here, we present a summary of the work to date on observations of photoelectrons at Venus, and their comparison with similar processes at Titan and Mars. We expand further by presenting new examples of the distant photoelectrons measured at Venus in the dark tail and further away from Venus than seen before. The photoelectron and simultaneous ion data are then used to determine the ion escape rate from Venus for one of these intervals. We compare the observed escape rates with other rates measured at Venus, and at other planets, moons and comets. We find that the escape rates are grouped by object type when plotted against body radius.

© 2015 The Authors. Published by Elsevier Ltd. This is an open access article under the CC BY license (http://creativecommons.org/licenses/by/4.0/).

1. Introduction

Photoionization by sunlight is the principal production process in many planetary ionospheres. As neutrals from the planetary atmospheres are ionized, ions and photoelectrons result. The solar spectrum, together with the composition of the atmosphere, provides photoelectrons with particular energies. The energy of the ionizing photon beyond the ionization potential of the gas gives the emerging photoelectron kinetic energy. In particular, there are peaks in the photoelectron spectrum in the 20–30 eV region, with particular energies for the various ionospheres. A summary of the expected peak energies for Venus, Earth, Mars and Titan is given by Coates et al. (2011) (see Table 1 in reference), based on theoretical ideas including Mantas and Hanson (1979) and Nagy and Banks (1970). The ionosphere is immersed in the Venus–solar wind interaction region, and in this paper we further investigate the interaction between the ionosphere and its environment.

A substantial amount of theoretical and simulation work has been done on the Venus–solar wind interaction, its ionosphere and the morphology of the interaction. On the large scale, the magnetic field configuration at Venus is due to the solar wind interaction with this unmagnetized planet (Luhmann, 1995). A bow shock, where the solar wind slows, is heated, and is deflected around the planet. The Interplanetary Magnetic Field (IMF) penetrates the shock and 'piles up' in front of the planet. The fields interact with the ionosphere as they drape around Venus (Luhmann and Cravens, 1991; Law and Cloutier, 1995). Several simulations have successfully reproduced the large scale features of the interaction, using both MHD (e.g. Ma et al., 2013) and hybrid (e.g. Brecht and Ferrante, 1991; Kallio and Jarvinen, 2012) models. The approaches were compared by Kallio et al. (2011).

Within the Venus ionosphere, the features unique to photo-electron energy spectra include sharp peaks in the primary photoelectron spectrum in the 20–30 eV range. These are from the ionization of neutrals by intense solar HeII 30.4 nm radiation. In addition, a reduction at ~ 60 eV is predicted due to a drop in the solar spectrum near 16 nm (e.g. Nagy and Banks, 1970; Mantas and Hanson, 1979; Fox, 2007). The peaks in this range are primarily produced by O rather than CO_2, because of the lower altitude of

* Corresponding author at: Mullard Space Science Laboratory, University College London, Holmbury St Mary, Dorking RH5 6NT, UK. Tel.: +44 1483 204145; fax: +44 1483 278312.
E-mail address: a.coates@ucl.ac.uk (A.J. Coates).

Table 1
Plasma loss estimates on 15 September 2009. Rates are in units of ions/s except where noted.

Observation date	E_{esc} H^+	E_{esc} $m=16$	E_{esc} $m=32$	V_{esc} $m=1$	V_{esc} $m=16$	Total	Mass loss (amu s^{-1})
15 Sep 09	8.2×10^{23}	2.1×10^{23}	1.0×10^{23}	1.0×10^{23}	1.2×10^{23}	2.2×10^{23}	2.0×10^{24}

the transition between CO_2 and O at Venus (Schunk and Nagy, 2000; Coates et al., 2008). The primary ionization process clearly introduces specific energy peaks in the energy spectrum (e.g. Gan et al., 1990; Cravens et al., 1980). These specific spectral features can be used to identify ionospheric photoelectrons.

A detailed comparison of a multi-stream kinetic model with ASPERA-ELS ionospheric photoelectron data was made by Cui et al. (2011). A good agreement was found between the observed and modelled photoelectron peak energies and flux decrease features, and fair agreement between the observed and modelled absolute fluxes was found when the magnetic field direction is included.

Observations of photoelectrons at Venus, Earth, Mars and Titan were summarized by Coates et al., (2011). At Venus, the first well-resolved measurements of ionospheric photoelectrons in the iono-sphere were given by Coates et al., 2008 using data from Venus Express. The flux of photoelectrons stayed fairly constant throughout the observation region in the Northern ionosphere, and from this it was inferred that the photoelectrons were produced during the ionization of oxygen at a lower altitude ($\sim$200 km) below the observation point (250–700 km). The observed photoelectrons were produced in the denser region of the atmosphere where atomic oxygen is abundant and then transported to the observation altitude.

One particular aspect of photoelectron observations, seen at all four objects, is the observations of ionospheric photoelectrons at locations well away from their production point, as well as locally in the ionosphere near the production point. These remote locations include the Earth's magnetosphere (at up to 6.6 R_E, Coates et al., 1985), in the Martian tail (at up to 3 R_M, Frahm et al., 2006a, 2006b; Coates et al., 2011), in Titan's tail (at up to 6.8 R_T, Coates et al., 2007; Wellbrock et al., 2012) where the observations were used to estimate ion loss rate (Coates et al., 2012), and at Venus (at up to 1.45–1.5 R_V, Tsang et al., accepted for publication; Coates et al., 2011). Tsang et al. (accepted for publication) also observed that at times near and beyond the terminator, the clear two-peak signature observed on the day side broadens into one peak, perhaps the result of scattering processes between the production and observation point (Jasperse, 1977; Jasperse and Smith, 1978). At Mars, photoelectron peaks were used to estimate the total loss rate of electrons from the Martian ionosphere, which was then suggested to be equal to the ion loss rate (Frahm et al., 2010). At Venus, escape rates appear to be dependent on upstream conditions (e.g. Brace et al., 1987, Barabash et al., 2007b; McEnulty et al., 2010).

In this paper, we present new case studies of photoelectrons seen in the Venus tail at larger distances than seen previously, and we make a new estimate of the ion escape flux from Venus using these measurements. We also summarize the observed plasma escape rates at various objects throughout the solar system as derived from in-situ measurements by spacecraft, and for the first time order these observed rates by body mass.

2. Instrumentation

We use data from the Electron Spectrometer (ELS) and the Ion Mass Analyzer (IMA), part of the Analyzer of Space Plasmas and Energetic Atoms (ASPERA-4) experiment on ESA's Venus Express (VEx) spacecraft (Barabash et al., 2007a). The ELS has an energy resolution of 8%, designed to provide well resolved measurements of photoelectrons at Venus (Barabash et al., 2007a; Coates et al., 2008).

3. Ionospheric photoelectrons in the Venus tail region

The first measurements of photoelectrons in the Venus tail region were given by Tsang et al., accepted for publication, which studied Venus Express data on 3, 4, and 30 June 2006, where photoelectrons were observed at 1.45 R_V in the tail region. An additional example with photoelectrons seen at 1.5 R_V on 20 April 2008 by Venus Express was shown by Coates et al. (2011). During this pass, photoelectrons were observed in the local ionosphere (interval A) as well as in the tail of Venus (interval B), and averaged spectra were shown from both intervals (Coates et al., 2011, Fig. 3). These tail photoelectrons were also associated with an increased flux of low energy ions. This led to the suggestion that polar wind-type escape along the draped magnetic field around Venus may be occurring, associated with an ambipolar electric field set up by relatively energetic photoelectrons (Hartle and Grebowsky, 1995; Coates et al., 2008, 2011).

Hybrid simulations of the Venus environment (Jarvinen et al., 2012) showed that draped fields with the suggested configuration were possible for suitable upstream conditions, at least early during interval B. Similar studies were done at Mars (Liemohn et al., 2006) and at Titan (Wellbrock et al., 2012). These simula-tions support the hypothesis that such field morphology is con-sistent with the observations.

We now present two new examples where ionospheric photo-electrons are seen in the tail: 8 May 2013 and 15 September 2009. These additional events are not the result of a full survey of the data, which is beyond the scope of the current paper. However, the two new events are measured (1) in the dark tail and (2) at larger distance along the tail, providing significant additional case studies.

3.1. 8 May 2013

Three types of plots are shown in Fig. 1. These are: the VEx orbital trajectory shown at the lower right, the ion and electron spectrogram at the lower left, and selected electron spectra at the top. Utilizing both the particle spectrograms and the orbital trajectory, VEx travels from the tail region (where intervals of relatively high energy solar wind halo/strahl electrons are seen, up to 0400 UT, and then again during an intensification at $\sim$0405 UT), through ionospheric plasma in the tail (before the terminator at $\sim$0425 UT) and then traversing the dayside ionosphere (0425-0431 UT), out to the magnetosheath (0431-0446 UT) then into the solar wind after the bow shock crossing at 0446 UT.

At various locations within the ionosphere, individual electron spectra highlight the observed distributions. The spectra A and B are measured before the terminator, with spectrum C measured just after the terminator. In all the spectra A, B and C, a broad peak structure in energy is observed between 10 and 20 eV, with some further detail also seen (2 peaks in spectra A and C in particular). We interpret the peaks in spectra A, B and C as due to ionospheric photoelectrons. Spectrum A in particular represents ionospheric photoelectrons observed in the dark tail region. Spectrum B appears somewhat broadened in energy; as found by Tsang et al. (accepted for publication), this may be due to scattering processes (Jasperse, 1977; Jasperse and Smith, 1978) between the production site in the dayside ionosphere and the observation site at the spacecraft. This may differ depending on which field line is being sampled.
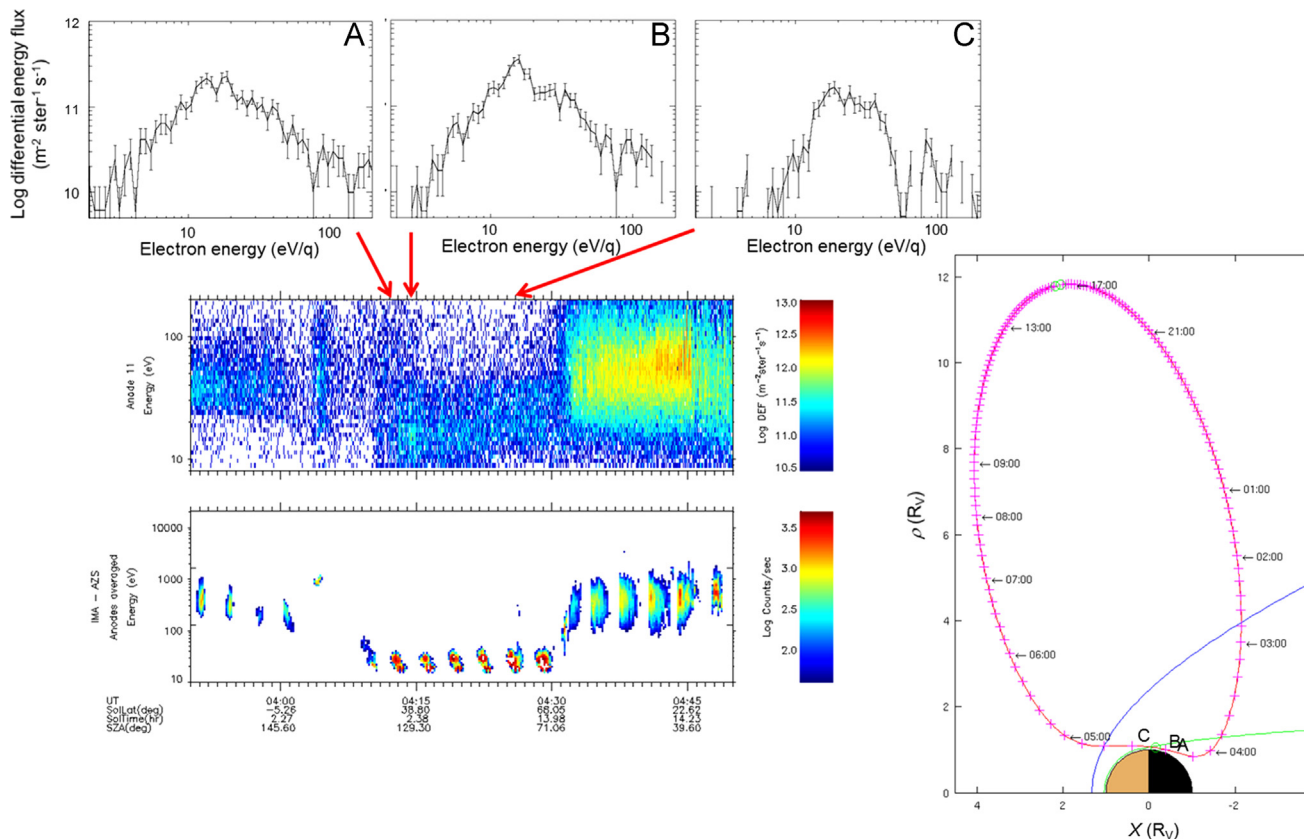
Fig. 1. Venus Express data on 8 May 2013. The spectrogram (lower left) includes ELS data (top) and ion data from IMA (bottom), with ELS spectra A,B and C from the time indicated by arrows. The orbit plot (right) indicates the locations of spectra A,B and C.

3.2. 15 September 2009

The data from 15 September 2009 are shown in Fig. 2. Here, the ELS spectrogram shows that the spacecraft starts in the tail region, as shown by the relatively energetic electrons, at up to ∼0145 UT. Intervals of ionospheric plasma are then observed at particular locations up to the terminator at ∼0226 UT. Sheath plasma is then observed after ∼0230 UT. The spectra A and B are shown from two of the intervals containing ionospheric plasma. Spectrum A is from ∼2 R_V along the tail while spectrum B is from the terminator. Both spectra show a two-peaked structure, highly reminiscent of the spectra in Coates et al., 2008. We interpret these observations as ionospheric photoelectrons. In the case of spectrum A, this observation is an example which is furthest away from the planet (about 2.3 R_V). It is important to note that the orbital constraints on VEx preclude observations further from the planet in the Venusian tail.

4. Venus ion escape rate estimate

For the 15 September 2009 case, we now estimate the escape rate along the Venusian tail, using a similar method to that discussed by Coates et al. (2012) at Titan. We estimate the flux of ions (Q) along the tail using the following equation:

$$Q = k n_{ELS} v A (\text{ions s}^{-1}) \qquad (1)$$

where $k = 2.9 \times 10^{22}$ (cm^3 km^{-1} R_c^{-2}) is a constant for units conversion, n_{ELS} (cm^{-3}) is the number density estimated from moment calculations of the ELS data, v is ion velocity relative to Venus (km s^{-1}) estimated from the peak of the ion spectrograms, and A is

the area (R_c^2) of the tail escape channel as a fraction of R_V (=6051 km), estimated from the duration of the ionospheric plasma seen near interval A. We have used an escape channel radius of 0.5 R_V in this calculation based on the time of observation of the iono-spheric photoelectrons on this particular orbit. By comparison with models, where larger and more complex escape channels are observed (e.g., Kallio et al. (2011), and references therein), the error on this area, and thus the escape rate estimate, could be at least 50%.

Since the parent ion from which electrons are liberated cannot be uniquely identified, the energy of the observed ion has been used to determine the ion velocity for H$^+$, O$^+$, and O$_2^+$. For each of these cases, the ion loss rates are shown in Table 1 in the columns indicated as E_{esc}.

Using IMA measurements of the ion velocity for H$^+$ and O$^+$ (not shown), we can make more accurate estimates of the loss rate, using these mass group-resolved data. These estimates are shown in the columns marked V_{esc}, for light (H$^+$) and heavy ions (O$^+$). These loss rates were calculated using Eq. (1).

Using the latter more accurate method, Table 1 shows in the Total column an estimated total loss rate of 2.2×10^{23} ions s^{-1} for this particular interval. Using the relative composition data this can be converted to a mass loss rate of 2.0×10^{24} amu s^{-1}.

We note that this estimate is lower than that provided in other studies (e.g., Barabash et al., 2007b). However, as mentioned above the error in this estimate could be as much as 50% due to possible uncertainties in the escape channel radius. In addition, not all of the tail is sampled by the Venus Express orbit, and it is possible that some of the escaping plasma is missed on each particular orbit. It is also worth pointing out that there will be differences in escape rate associated with different upstream conditions as well as solar cycle variations.
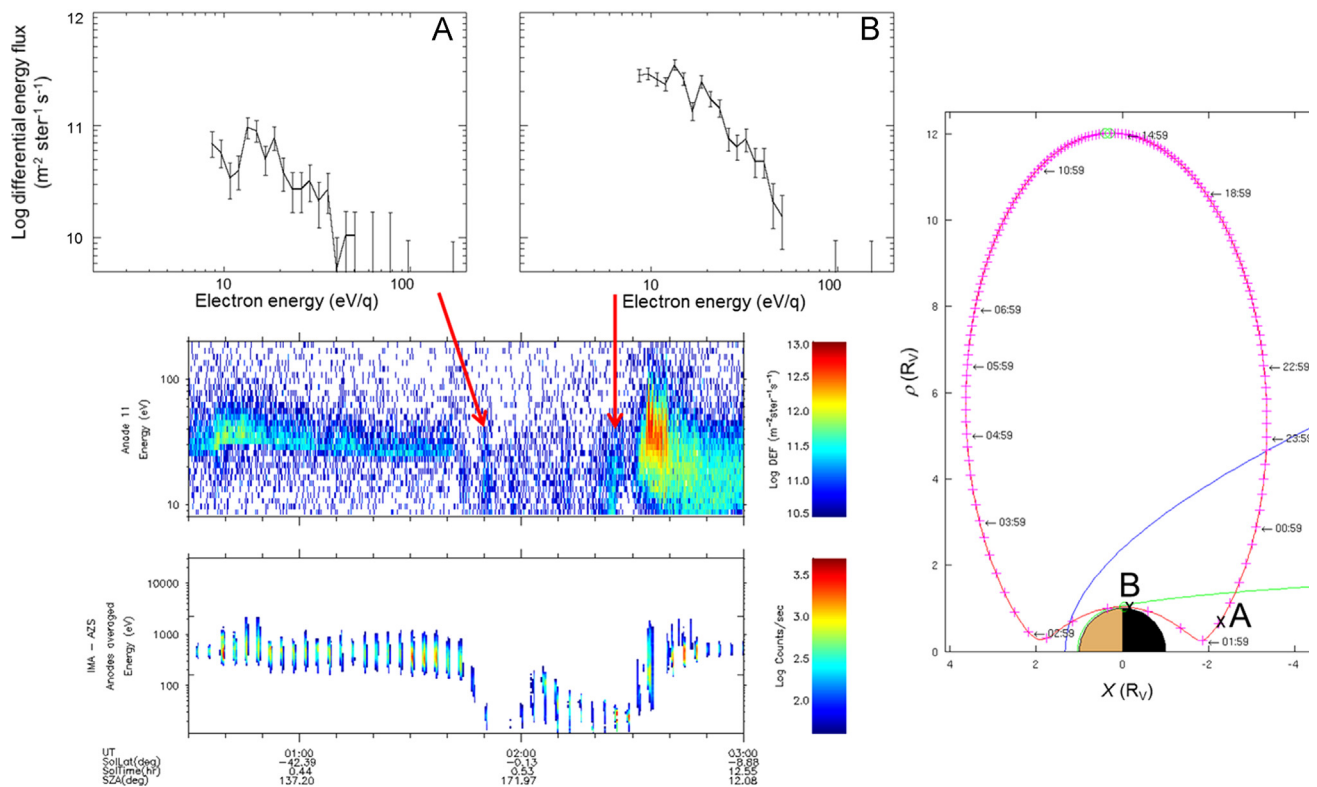
Fig. 2. Venus Express data from 15 September 2009. Format as for Fig. 1, except that two spectra A and B are shown.

Table 2
Neutral gas production rates for comets and other solar system objects visited by spacecraft with plasma instrumentation.

Comet	Spacecraft	Production rate (molecules s^{-1})	Ratio (Halley=100)	Reference
Giacobini–Zinner (GZ)	ICE	4×10^{28}	5.8	(Mendis et al., 1986)
Halley	Giotto, Vega, Suisei, Sakigake	6.9×10^{29}	100	(Krankowsky et al., 1986)
Grigg–Skjellerup (GS)	Giotto (GEM)	7.5×10^{27}	1.1	(Johnstone et al., 1993)
Borrelly	DS1	3.5×10^{28}	5.1	(Young et al., 2004)
Churyumov–Gerasimenko (CG)	Rosetta (2014–2015)	3×10^{24}–5×10^{27}	4.3×10^{-4}–0.7	(Hansen et al., 2007; Motschmann and Kührt, 2006)
Mercury	Ground-based (Na)	10^{24}–10^{25}	1.5×10^{-4}–1.5×10^{-3}	(Potter et al., 2002)
Venus	VEx, PVO	[a]2.2×10^{23}–10^{25}	3×10^{-5}–1.5×10^{-3}	(This work 15, Brace et al., 1987; Barabash et al., 2007b)
Mars	MEx, Phobos	[a]10^{23}–10^{25}	1.5×10^{-5}–1.5×10^{-3}	(Barabash et al., 2007c; Lundin et al., 2008; Lundin et al., 2013; Lundin et al., 1989; Ramstad et al., 2013)
Io	Galileo	3×10^{28}	4.3	(Bagenal, 1994)
Europa	Galileo	2×10^{27}	0.29	(Smyth and Marconi 2006)
Ganymede	Galileo	1.3×10^{27}	0.19	(Marconi, 2007)
Titan	Cassini	[a]4×10^{24}–10^{25}	1–1.5×10^{-3}	(Coates et al., 2012; Wahlund et al., 2005)
Enceladus	Cassini	3×10^{27} to 1–2×10^{28}	0.43–2.9	(Tokar et al., 2006)
Enceladus L-shell	Cassini	3.8–7.6×10^{26}	0.06–0.12	(Cowee et al., 2009)
Rhea	Cassini	2.45×10^{24}	3.6×10^{-4}	(Teolis et al., 2010)

[a] Ion loss rate estimates.

5. Venus escape rate compared to other solar system bodies

To compare the estimated escape rate in the previous section with other estimates at solar system objects in general, including planets, comets and moons, we have assembled some of the estimates of production and escape rates made over the last few years, primarily from spacecraft observations. The results are summarized in Table 2 (adapted from Coates, 2012).

We now take these estimates and compare them with the radius of the appropriate object. In Fig. 3, we show the rates plotted as a function of body radius. Remarkably, three broad groups appear when plotting the data in this way – planets, moons and comets. The planet and moons groups overlap to some extent as seen in Fig. 3. We should point out that for all objects the rates are in reality time dependent – for comets, for example, the rate will be dependent on heliocentric distance, and for all objects the rates will depend on
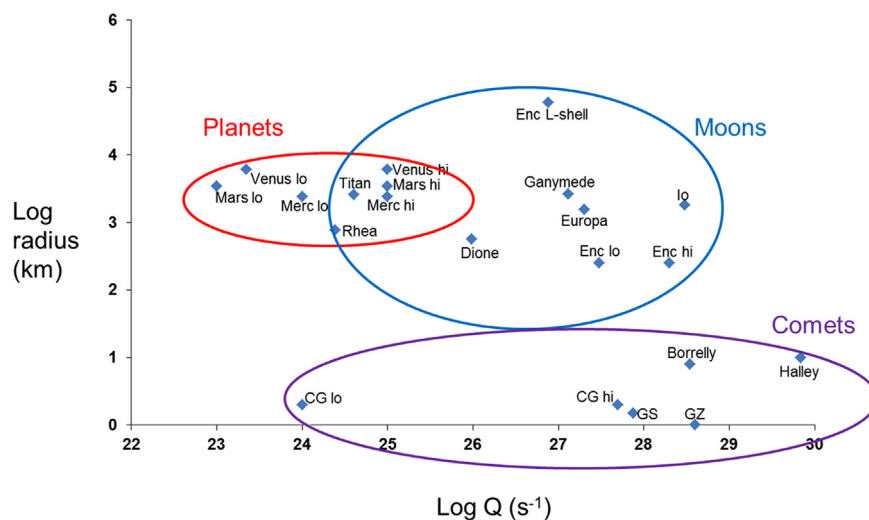
Fig. 3. Collection of measured production rates from solar system objects (Table 2), plotted as a function of object radius.
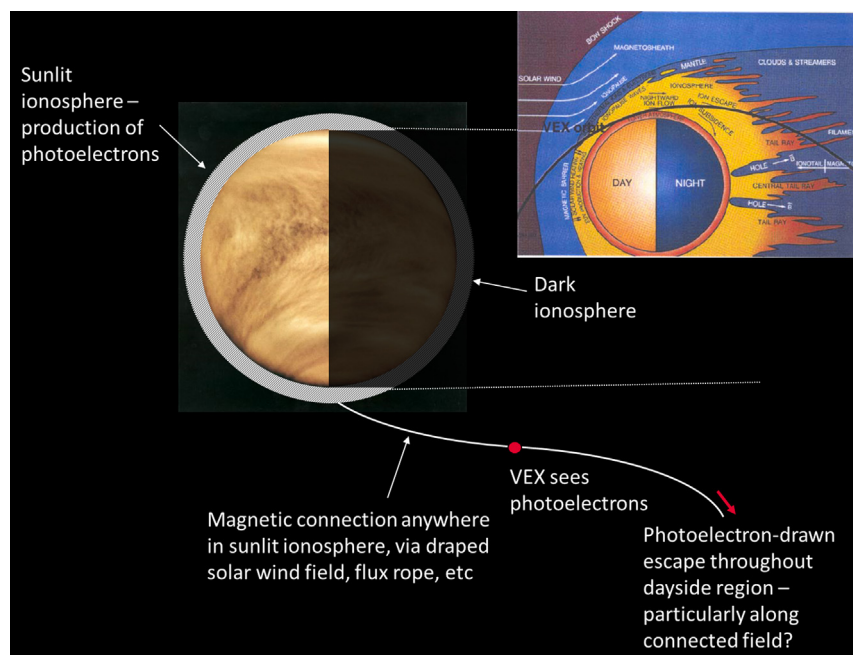

Fig. 4. Schematic of the observation of photoelectrons in the Venus tail. The magnetic connection between the ionosphere and the observation point is shown. The inset plot (Brace et al., 1987, with a representative Venus Express trajectory overlaid) shows the possible extension of ionosphere into the tail.

upstream conditions and on solar cycle effects. These factors will introduce some additional variation beyond that shown.

6. Summary and conclusions

Regarding photoelectrons at Venus, we can summarize the results presented here as follows:

- On 8 May 2013, photoelectrons are seen in the dark tail region where production by sunlight is certainly absent. This is indicative of transport to this observation point, probably along a draped field line connected to the ionosphere (as modelled at Mars by Liemohn et al., at Titan by Sillanpaa et al., and presented in Wellbrock et al., 2012). A preliminary study by Jarvinen et al. (2012) showed that it was indeed possible for photoelectrons to be picked-up by draped magnetic field lines as in the Coates et al. (2011) event.

- On 15 September 2009, photoelectrons are seen at $\sim 2.3\ R_V$, the largest distance that ionospheric photoelectrons, originating in Venus' sunlit ionosphere, have been observed along the Venus tail to date. Again, this indicates a magnetic connection as local production would be absent due to the lack of ionizing sun light.

The examples of photoelectrons in the Venus tail region presented in this paper, together with the earlier observations from Coates et al. (2008), Tsang et al. (accepted for publication), and Coates et al. (2011), show that photoelectrons at Venus may be observed at remote locations from their production point in the dayside ionosphere. As at Titan (Coates et al., 2007; Wellbrock et al., 2012), Mars (Frahm et al., 2006a, 2006b) and the Earth (Coates et al., 1985), this is indicative of a magnetic connection between the ionosphere and the observation point. This is summarized in Fig. 4 for Venus.

The presence of photoelectrons in the tail, together with low-energy ions, is possible evidence for a polar wind style escape at

Venus. The relatively energetic electrons set up an ambipolar electric field which draws ions out of the ionosphere. This mechanism may supplement any escape due to pickup ions (e.g. Luhmann et al., 2008, as well as from ionospheric outflow, e.g. Fedorov et al., 2008).

The result of the escape calculation presented here is a little lower than earlier estimates, but such estimates are very sensitive to the assumed area of the escape channel. While the diameter of this is determined by observations, its shape may well differ from the assumed cylindrical shape. Different shapes have been seen in simulations at unmagnetized objects (e.g. Ma and Nagy, 2007; Snowden and Winglee, 2013).

To our knowledge, Fig. 3 presents the first time that the escape rates of all of these classes of objects have been gathered and plotted in this way. The escape rates for other solar system objects show a remarkable grouping of rates for planets, moons and comets, when the escape rate is plotted against body radius. In general, the escape rates are higher for smaller sized objects – this is visible for both the comets and for the moons when compared with planets. Although the body mass clearly plays a role in stopping thermal ion escape, and this is consistent with the observations, additional escape processes are underway (including bulk ionospheric escape and photoelectron driven escape).

Clearly, there are different escape processes at work for all objects, including thermal and non-thermal mechanisms, which contribute to all of the points. Nevertheless, some interesting trends emerge. The relatively small objects, i.e. the comets, have generally higher escape rates, likely due to their lower gravity. The moons shown are generally higher escape rates for similar size objects, in the cases of Io and Enceladus due to their intrinsic activity, and in the other cases shown because of their immersion in hot magnetospheres rather than the solar wind.

Significant modelling efforts, as well as experimental studies, are underway to understand the different escape rates at different objects. Understanding the complex escape processes are important for determining atmospheric evolution, and for determining the history of volatiles in the solar system.

Acknowledgments

References

Bagenal, F., 1994. Empirical model of the Io plasma torus: Voyager measurements. J. Geophys. Res. 99, 11043–11062.

Barabash, S., Sauvaud, J.-A., Gunell, H., Andersson, H., Grigoriev, A., Brinkfeldt, K., Holmström, M., Lundin, R., Yamauchi, M., Asamura, K., Baumjohann, W., Zhang, T., Coates, A.J., Linder, D.R., Kataria, D.O., Curtis, C.C, Hsieh, K.C., Sandel, B.R., Fedorov, A., Mazelle, C., Thocaven, J.-J., Grande, M., Koskinen, Hannu E.J., Kallio, E., Säles, T., Riihela, P., Kozyra, J., Krupp, N., Woch, J., Luhmann, J., McKenna-Lawlor, S., Orsini, S., Cerulli-Irelli, R., Mura, M., Milillo, M., Maggi, M., Roelof, E., Brandt, P., Russell, C.T., Szego, K., Winningham, J.D., Frahm, R.A., Scherrer, J., Sharber, J.R., Wurz, P., Bochsler, P., 2007a. The analyser of space plasmas and energetic atoms (ASPERA-4) for the Venus Express mission. Planet. Space Sci. 55, 1772–1792.

Barabash, S., Fedorov, A., Sauvaud, J.A., Lundin, R., Russell, C.T., Futaana, Y., Zhang, T.L., Andersson, H., Brinkfeldt, K., Grigoriev, A., Holmström, M., Yamauchi, M., Asamura, K., Baumjohann, W., Lammer, H., Coates, A.J., Kataria, D.O., Linder, D.R., Curtis, C.C., Hsieh, K.C., Sandel, B.R., Grande, M., Gunell, H., Koskinen, H.E.J., Kallio, E., Riihela, P., Säles, T., Schmidt, W., Kozyra, J., Krupp, N., Fränz, M., Woch, J., Luhmann, J., McKenna-Lawlor, S., Mazelle, C., Thocaven, J.-J., Orsini, S., Cerulli-Irelli, R., Mura, M., Milillo, M., Maggi, M., Roelof, E., Brandt, P., Szego, K., Winningham, J.D., Frahm, R.A., Scherrer, J., Sharber, J.R., Wurz, P., Bochsler, P., 2007b. The loss of ions from Venus through the plasma wake. Nature 450, 650–653.

Barabash, S., Fedorov, A., Lundin, R., Sauvaud, J.-A., 2007c. Martian atmospheric erosion rates. Science 315, 501–503.

Brace, L.H., Kasprzak, W.T., Taylor, H.A., Theis, R.F., Russell, C.T., Barnes, A., Mihalov, J.D., Hunten, D.M., 1987. The ionotail of Venus – its configuration and evidence for ion escape. J. Geophys. Res. 92, 15–26.

Brecht, S.H., Ferrante, J.R., 1991. J. Geophys. Res. 96, 11209–11220.

Coates, A.J., 2012. Ion pickup and acceleration: measurements from planetary missions, In: Heerikhuisen, Jacob, Li, Gang, Pogorelov, Nikolai, Zank, Gary (Eds.), Proceedings of the 10th Annual Astrophysics Conference 'Physics of the heliosphere: a 10-year retrospective', AIP Conf. Proc. 1436, 89–102.

Coates, A.J., Johnstone, A.D., Johnson, J.F.E., Sojka, J.J., Wrenn, G.L., 1985. Ionospheric photoelectrons observed in the magnetosphere at distances of up to 7 Earth radii. Planet. Space Sci. 33, 1267–1275.

Coates, A.J., Crary, F.J., Young, D.T., Szego, K., Arridge, C.S., Bebesi, Z., Sittler Jr., E.C., Hartle, R.E., Hill, T.W., 2007. Ionospheric electrons in Titan's tail: plasma structure during the Cassini T9 encounter. Geophys. Res. Lett. 34, L24S05.

Coates, A.J., Frahm, R.A., Linder, D.R., Kataria, D.O., Soobiah, Y., Collinson, G., Sharber, J.R., Winningham, J.D., Jeffers, S.J., Barabash, S., Sauvaud, J.–A., Lundin, R., Holmström, M., Futaana, Y., Yamauchi, M., Grigoriev, A., Andersson, H., Gunell, H., Fedorov, A., Thocaven, J.–J., Zhang, T., Baumjohann, W., Kallio, E., Koskinen, H., Kozyra, J.U., Liemohn, M.W., Ma, Y., Galli, A., Wurz, P., Bochsler, P., Brain, D., Roelof, E.C., Brandt, P., Krupp, N., Woch, J., Fraenz, M., Dubinin, E., McKenna-Lawlor, S., Orsini, S., Cerulli-Irelli, R., Mura, A., Milillo, A., Maggi, M., Curtis, C.C., Sandel, B.H., Hsieh, K.C., Szego, K., Asamura, A., Grande, M., 2008. Ionospheric photoelectrons at Venus: initial observations by ASPERA-4 ELS. Planet. Space Sci. 56, 802–806.

Coates, A.J., Tsang, S.M.E., Wellbrock, A., Frahm, R.A., Winningham, J.D., Barabash, S., Lundin, R., Young, D.T., Crary, F.J., 2011. Ionospheric photoelectrons: comparing Venus, Earth, Mars and Titan. Planet. Space Sci. 59, 1019–1027.

Coates, A.J., Wellbrock, A., Lewis, G.R., Arridge, C.S., Crary, F.J., Young, D.T., Thomsen, M.F., Reisenfeld, D.B., Sittler Jr, E.C., Johnson, R.E., Szego, K., Bebesi, Z., Jones, G.H., 2012. Cassini in Titan's tail: CAPS observations of plasma escape. J. Geophys. Res. 117, A05324.

Cowee, M.M., Omidi, N., Russell, C.T., Blanco-Cano, X., Tokar, R.L., 2009. Determining ion production rates near Saturn's extended neutral cloud from ion cyclotron wave amplitudes. J. Geophys. Res. 114, A04219.

Cravens, T.E., Gombosi, T.I., Kozyra, J., Nagy, A.F., Brace, L.H., Knudsen, W.C., 1980. Model calculations of the dayside ionosphere of Venus: Energetics. J. Geophys. Res. 85, 7778–7786.

Cui, J., Galand, M., Coates, A.J., Zhang, T.L., Müller-Wodarg, I.C.F, 2011. Suprathermal electron spectra in the Venus ionosphere. J. Geophys. Res. 116, A04321. http://dx.doi.org/10.1029/2010JA016153.

Fedorov, A., Ferrier, C., Sauvaud, J.A., Barabash, S., Zhang, T.L., Mazelle, C., Lundin, R., Gunell, H., Andersson, H., Brinkfeldt, K., Futaana, Y., Grigoriev, A., Holmström, M., Yamauchi, M., Asamura, K., Baumjohann, W., Lammer, H., Coates, A.J., Kataria, D. O., Linder, D.R., Curtis, C.C., Hsieh, K.C., Sandel, B.R., Thocaven, J.-J., Grande, M., Koskinen, H., Kallio, E., Sales, T., Schmidt, W., Riihela, P., Kozyra, J., Krupp, N., Woch, J., Luhmann, J., McKenna-Lawlor, S., Orsini, S., Cerulli-Irelli, R., Mura, A., Milillo, A., Maggi, M., Roelof, E., Brandt, P., Russell, C.T., Szego, K., Winningham, J. D., Frahm, R.A., Scherrer, J., Sharber, J.R., Wurz, P., Bochsler, P., 2008. Comparative analysis of Venus and Mars magnetotails. Planet. Space Sci. 56, 812–817.

Fox, J.L., 2007. Near-terminator Venus ionosphere: how Chapman-esque? J. Geophys. Res. 112, E04S02.

Frahm, R.A., Winningham, J.D., Sharber, J.R., Scherrer, J.R., Jeffers, S.J., Coates, A.J., Linder, D.R., Kataria, D.O., Lundin, R., Barabash, S., Holmström, M., Andersson, H., Yamauchi, M., Grigoriev, A., Kallio, E., Koskinen, H., Säles, T., Riihela, P., Schmidt, W., Kozyra, J.U., Luhmann, J.G., Roelof, E.C., Williams, D.J., Livi, S., Curtis, C.C., Hsieh, K.C., Sandel, B.R., Grande, M., Carter, M., Sauvaud, J.-A., Fedorov, A., Thocaven, J.-J., McKenna-Lawlor, S., Orsini, S., Cerulli-Irelli, R., Maggi, M., Wurz, P., Bochsler, P., Krupp, N., Woch, J., Fraenz, M., Asamura, K., Dierker, C., 2006a. Carbon dioxide photoelectron peaks at Mars. Icarus 182, 371–382.

Frahm, R.A., Sharber, J.R., Winningham, J.D., Wurz, P., Liemohn, M.W., Kallio, E., Yamauchi, M., Lundin, R., Barabash, S., Coates, A.J., Linder, D.R., Kozyra, J.U., Holmström, M., Jeffers, S.J., Andersson, H., McKenna-Lawlor, S., 2006b. Locations of atmospheric photoelectron energy peaks within the Mars environment. Space Sci. Rev. 126, 389–402.

Frahm, R.A., Sharber, J.R., Winningham, J.D., Link, R., Liemohn, M.W., Kozyra, J.U., Coates, A.J., Linder, D.R., Barabash, S., Lundin, R., Fedorov, A., 2010. Estimation of the escape of photoelectrons from Mars in 2004 liberated by the ionization of carbon dioxide and atomic oxygen. Icarus 206, 50–63.

Gan, L., Cravens, T.E., Horanyi, M., 1990. Electrons in the ionopause boundary layer of Venus. J. Geophys. Res. 95 (A11), 19023–19035.

Hansen, K.C., Bagdonat, T., Motschmann, U., Alexander, C., Combi, M.R., Cravens, T.E., Gombosi, T.I., Jia, Y.-D., Robertson, I.P., 2007. The plasma environment of comet 67P/Churyumov–Gerasimenko throughout the Rosetta main mission. Space Sci. Rev. 128, 133–166.

Hartle, R.E., Grebowsky, J.M., 1995. Planetary loss from light ion escape on Venus. Adv. Space Res. 15, 117–122.

Jarvinen, R., A.J. Coates, T.L. Zhang, S. Barabash, A. Fedorov, E. Kallio, 2012. Magnetic connectivity and photoelectrons in the Venus plasma environment, In: Proceedings of the European Planetary Science Congress, 23–28 September, Madrid, Spain.

Jasperse, J.R., 1977. Electron distribution function and ion concentrations in the Earth's lower ionosphere from Boltzmann–Fokker–Planck theory. Planet. Space Sci. 25, 743–756. http://dx.doi.org/10.1016/0032-0633(77)90126-X.

Jasperse, J.R., Smith, E.R., 1978. The photoelectron flux in the Earth's ionosphere at energies in the vicinity of photoionization peaks. Geophys. Res. Lett. 5, 843–846.

Johnstone, A.D., Coates, A.J., Huddleston, D.E., Jockers, K., Wilken, B., Borg, H., Gurgiolo, C., Winningham, J.D., Amata, E., 1993. Observations of the solar wind and cometary ions during the encounter between giotto and comet Grigg-Skjellerup. Astron. Astrophys. 273, L1–L4.

Kallio, E., Chaufray, J.-Y., Modolo, R., Snowden, D., Winglee, R., 2011. Modeling of Venus, Mars, and Titan. Space Sci. Rev. 162, 267–307.

Kallio, E., Jarvinen, R., 2012. Kinetic effects on ion escape at Mars and Venus: hybrid modeling studies. Earth, Planets Space 64, 157–163.

Krankowsky, D., Lammerzahl, P., Herrwerth, I., Woweries, J., Eberhardt, P., Dolder, U., Herrmann, U., Schulte, W., Berthelier, J.-J., Illiano, J.M., Hodges, R.R., Hoffman, J.H., 1986. In situ gas and ion measurements at comet Halley. Nature 321, 326–329.

Law, C.C., Cloutier, P.A., 1995. Observations of magnetic structure at the dayside ionopause of Venus. J. Geophys. Res. 100, 23973–23981.

Liemohn, M.W., Ma, Y., Frahm, R.A., Fang, X., Kozyra, J.U., Nagy, A.F., Winningham, J.D., Sharber, J.R., Barabash, S., Lundin, R., 2006. Mars global MHD predictions of magnetic connectivity between the dayside ionosphere and the magnetospheric flanks. Space Sci. Rev. 126, 63–76.

Luhmann, J.G., 1995. Plasma interactions with unmagnetized bodies. In: Kivelson, M.G., Russell, C.T. (Eds.), Introduction to Space Physics. Cambridge University Press, Cambridge, pp. 203–226.

Luhmann, J.G., Cravens, T.E., 1991. Magnetic fields in the ionosphere of Venus. Space. Sci. Rev. 55 (1–4), 201–274.

Luhmann, J.G., Fedorov, A., Barabash, S., Carlsson, E., Futaana, Y., Zhang, T.L., Russell, C.T., Lyon, J.G., Ledvina, S.A., Brain, D.A., 2008. Venus Express observations of atmospheric oxygen escape during the passage of several coronal mass ejections. J. Geophys. Res. 113, E00B0.

Lundin, R., Borg, H., Hultqvist, B., Zakharov, A., Pellinen, R., 1989. First measurements of the ionospheric plasma escape from Mars. Nature 341, 609–612.

Lundin, R., Barabash, S., Holmström, M., Nilsson, H., Yamauchi, M., Fraenz, M., Dubinin, E.M., 2008. A comet-like escape of ionospheric plasma from Mars. Geophys. Res. Lett. 35, L18203.

Lundin, R., Barabash, S., Holmström, M., Nilsson, H., Futaana, Y., Ramstad, R., Yamauchi, M., Dubinin, E., Fraenz, M., 2013. Solar cycle effects on the ion escape from Mars. Geophys. Res. Lett. 40, 6028–6032.

Ma, Y.-J., Nagy, A.F., 2007. Ion escape fluxes from Mars. Geophys. Res. Lett. 34, L0820.

Ma, Y.J., Nagy, A.F., Russell, C.T., Strangeway, R.J., Wei, H.Y., Toth, G., 2013. A global multispecies single-fluid MHD study of the plasma interaction around Venus. J. Geophys. Res.: Space Phys. 118, 321–330.

Mantas, G.P., Hanson, W.B., 1979. Photoelectron fluxes in the Martian ionosphere. J. Geophys. Res 84, 369–385.

Marconi, M.L., 2007. A kinetic model of Ganymede's atmosphere. Icarus 190, 155–174.

McEnulty, T.R., Luhmann, J.G., de Pater, I., Brain, D.A., Fedorov, A., Zhang, T.L., E. Dubinin, E., 2010. Interplanetary coronal mass ejection influence on high energy pick-up ions at Venus. Planet. Space. Sci. 58, 1784–1791.

Mendis, D.A., Smith, E.J., Tsurutani, B.T., Slavin, J.A., Jones, D.E., Siscoe, G.L., 1986. Comet-solar wind interaction: dynamical length scales and models. Geophys. Res. Lett. 13, 239–242.

Motschmann, U., Kührt, E., 2006. Interaction of the solar wind with weak obstacles: hybrid simulations for weakly active comets and for Mars. Space Sci. Rev. 122, 197–208.

Nagy, A.F., Banks, P.M., 1970. Photoelectron fluxes in the ionosphere. J. Geophys. Res. 75, 6260–6270.

Potter, A.E., Killen, R.M., Morgan, T.H., 2002. The sodium tail of Mercury. Meteorit. Planet. Sci. 37, 1165–1172.

Ramstad, R., Futaana, Y., Barabash, S., Nilsson, H., Martin Del Campo B, S., Lundin, R., Schwingenschuh, K., 2013. Phobos 2/ASPERA data revisited: planetary ion escape rate from Mars near the 1989 solar maximum. Geophys. Res. Lett. 40, 477–481.

Schunk, R.W., Nagy, A.F., 2000. Ionospheres – Physics, Plasma Physics, and Chemistry. Cambridge University Press, pp. 433–443.

Smyth, W.H., Marconi, M.L., 2006. Europa's atmosphere, gas tori, and magnetospheric implications. Icarus 181, 510–526.

Snowden, D., Winglee, R., 2013. Three-dimensional multi-fluid simulations of Titan's interaction with Saturn's magnetosphere: comparisons with cassini's T55 flyby. J. Geophys. Res. 118, 4852–4863.

Teolis, B.D., Jones, G.H., Miles, P.F., Tokar, R.L., Magee, B.A., Waite, J.H., Roussos, E., Young, D.T., Crary, F.J., Coates, A.J., Johnson, R.E., Tseng, W.-L., Baragiola, R.A., 2010. Cassini finds an oxygen–carbon dioxide atmosphere at Saturn's icy moon Rhea. Science 330, 1813–1815.

Tokar, R.L., Johnson, R.E., Hill, T.W., Pontius, D.H., Kurth, W.S., Crary, F.J., Young, D.T., Thomsen, M.F., Reisenfeld, D.B., Coates, A.J., Lewis, G.R., Sittler, E.C., Gurnett, D. A., 2006. The Interaction of the atmosphere of enceladus with Saturn's plasma. Science 311, 1409–1412.

Tsang S.M.E., Coates A.J., Jones G.H., Frahm R.A., Winningham J.D., Barabash S., Lundin R., Fedorov A., Ionospheric photoelectrons at Venus: case studies and first observation in the tail, Planet. Space Sci. http://dx.doi.org/10.1016/j.pss.2015.01.019 (accepted for publication).

Wahlund, J.-E., Boström, R., Gustafsson, G., Gurnett, D.A., Kurth, W.S., Pedersen, A., Averkamp, T.F., Hospodarsky, G.B., Persoon, A.M., Canu, P., Neubauer, F.M., Dougherty, M.K., Eriksson, A.I., Morooka, M.W., Gill, R., André, M., Eliasson, L., Müller-Wodarg, I., 2005. Cassini measurements of cold plasma in the ionosphere of Titan. Science 308, 986–989.

Wellbrock, A., Coates, A.J., Sillanpää, I., Jones, G.H., Arridge, C.S., Lewis, G.R., Young, D.T., Crary, F.J., Aylward, A.D., 2012. Cassini observations of ionospheric photoelectrons at large distances from Titan: implications for Titan's exospheric environment and magnetic tail. J. Geophys. Res. 117, A03216.

Young, D.T., Crary, F.J., Nordholt, J.E., Bagenal, F., Boice, D., Burch, J.L., Eviatar, A., Goldstein, R., Hanley, J.J., Lawrence, D.J., McComas, D.J., Meier, R., Reisenfeld, D., Sauer, K., Wiens, R.C., 2004. Solar wind interactions with comet 19P/Borrelly. Icarus 167, 80–88.